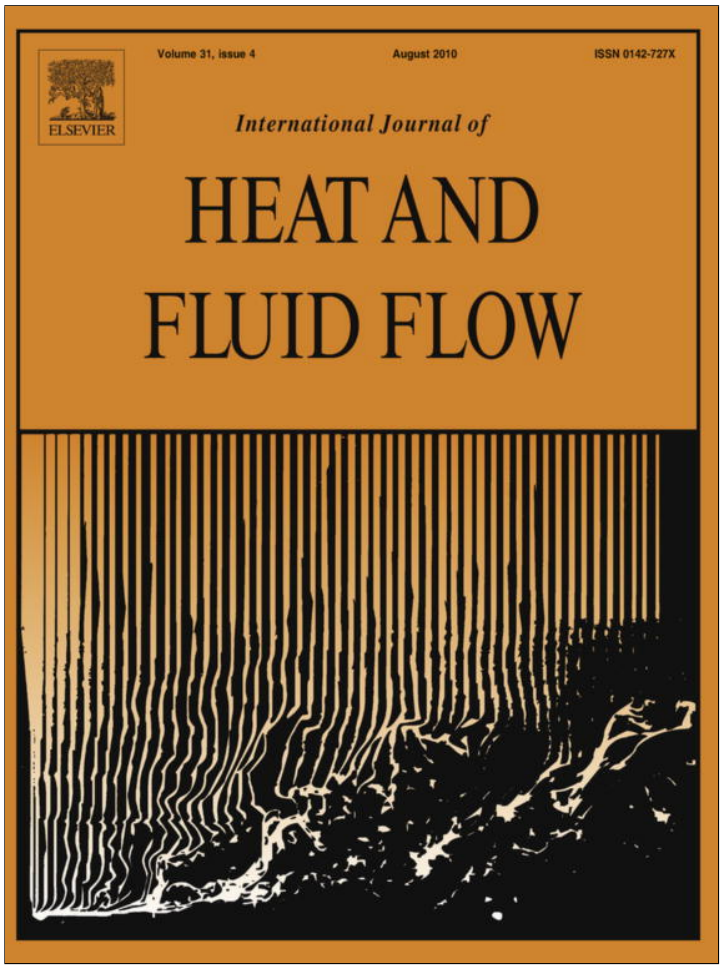

International Journal of Heat and Fluid Flow 31 (2010) 499–506

Contents lists available at ScienceDirect

International Journal of Heat and Fluid Flow

journal homepage: www.elsevier.com/locate/ijhff

Very fine near-wall structures in turbulent scalar mixing

L. Galantucci, M. Quadrio *

Dip. Ingegneria Aerospaziale, Politecnico di Milano via La Masa, 34, 20156 Milano, Italy

ARTICLE INFO

Article history:
Received 9 October 2009
Received in revised form 24 March 2010
Accepted 3 April 2010
Available online 5 May 2010

Keywords:
Turbulence
Passive scalar
Channel flow
Spatial resolution

ABSTRACT

Passive scalar dynamics in wall-bounded turbulence is studied via Direct Numerical Simulations of plane channel flow, for a friction Reynolds number $Re_* = 160$ and a Schmidt number $Sc = 1$. Peculiar to the present research is that the spatial resolution reaches beyond what has been employed in similar past studies. Our aim is to examine the statistics of the most dissipative events across the various layers of the channel flow, and to compare them to the homogeneous isotropic case, where the recent studies by Schumacher et al. (2005) and Watanabe and Gotoh (2007) have described a range of scalar micro-scales that require extremely high spatial resolution to be properly resolved.

Resolution effects are observed on integral-scale (non-local) quantities such as the mean profiles of the scalar dissipation and its variance. By examining probability distributions, it is found that the finest resolution is essential for correctly computing small-scale statistics in the near-wall region of the channel. As expected, this high-resolution requirement extends outwards to the channel centerline, where the behaviour of isotropic turbulence is recovered. However, marginal resolution, that underemphasizes high-intensity scalar dissipation events in the nearly-isotropic central region, is found to overemphasize them significantly near the wall.

1. Introduction

A passive scalar in a fluid flow is a diffusive physical quantity whose dynamical effects on the velocity field can be neglected. Examples of quantities that can often be conveniently treated as passive scalars are pollutants in liquids and gases, moisture in air, temperature in heated fluids (provided temperature fluctuations are sufficiently small), dye in liquids, chemical reactant species in industrial processes, etc. A comprehensive review of the literature on passive scalars and turbulence is given by Warhaft (2000).

The turbulent mixing of a passive scalar arises from two different yet concurring mechanisms: advective dispersion by large-scale motions and small-scale diffusive molecular mixing. Experimental results (Warhaft, 2000) as well as Direct Numerical Simulations (Brethouwer et al., 2003) show that these two physical processes are strongly coupled. As a consequence, a precise knowledge of the scalar's smallest scales is required for studying its integral-scale properties, such as the mean profile, the transport, the production and dissipation rates of scalar variance and the scalar flux.

Understanding the smallest scales of scalar motion plays a key role in modeling the budget equation for the scalar variance, which is of interest in the LES and RANS approaches to turbulent flows. A satisfactory knowledge of the smallest scales might also improve our understanding of turbulence as a whole, as discussed by Shraiman and Siggia (2000). Despite the linearity of the advection–diffusion equation with respect to the scalar, considerable internal intermittency and small-scale anisotropy characterize the passive scalar field (Sreenivasan, 1991; Sreenivasan and Antonia, 1997), and are larger than the ones of the corresponding turbulent velocity field (Chen and Cao, 1997; Mydlarski and Warhaft, 1998; Wang et al., 1999; Warhaft, 2000; Yeung et al., 2005).

An effective tool for the numerical study of the smallest features of scalar motions is the Direct Numerical Simulation (DNS) of the Navier–Stokes equations coupled to the passive scalar's advection–diffusion equation. To obtain reliable and accurate results, however, an adequate spatial resolution must be chosen in order to resolve all the significant scales of motion.

The typical lengthscale of the smallest scalar motions is the mean Batchelor length scale $\langle \eta_B \rangle$, given by the mean Kolmogorov length scale $\langle \eta \rangle$ divided by the square root of the Schmidt number $Sc = \nu/\gamma$:

$$\langle \eta_B \rangle = \frac{\langle \eta \rangle}{Sc^{1/2}}, \tag{1}$$

where ν is the kinematic viscosity of the fluid and γ is the scalar diffusivity; the operator $\langle \cdot \rangle$ denotes an average taken over homogeneous directions and time.

* Corresponding author.
E-mail addresses: galantucci@aero.polimi.it (L. Galantucci), maurizio.quadrio@polimi.it (M. Quadrio).

0142-727X/$ - see front matter © 2010 Elsevier Inc. All rights reserved.
doi:10.1016/j.ijheatfluidflow.2010.04.002

However, the fact that, on average, the smallest scales of the scalar motions are given by $\langle\eta_B\rangle$ does not imply that a spatial resolution set at $\langle\eta_B\rangle$ is sufficient. This consideration has recently led several authors (Sreenivasan, 2004; Yakhot and Sreenivasan, 2005; Schumacher et al., 2007) to suggest more stringent spatial resolution requirements for the adequate representations of velocity statistics in DNS of homogeneous and isotropic turbulence. In particular, Donzis et al. (2008) introduced a criterion that provides an error estimate as a function of small-scale resolution.

The proper spatial resolution for the DNS of passive scalars has been recently addressed by Schumacher et al. (2005) and Watanabe and Gotoh (2007) in the context of homogeneous and isotropic turbulence. The general conclusions of the two papers are similar: they point to the existence and dynamical relevance of scalar micro-scales that would be misrepresented, should one set the spatial resolution of the numerical simulation based on $\langle\eta_B\rangle$. In fact, they demonstrate how the value of η_B may become very small locally, and establish that in such cases scales larger than η_B and smaller than $\langle\eta_B\rangle$ must be represented in the numerical simulation for the small-scale statistics to be correctly predicted.

In particular, Schumacher et al. (2005) examined how these micro-scales in homogeneous isotropic turbulence behave as the Schmidt number is increased, whereas Watanabe and Gotoh (2007) used the computing power of the Earth Simulator to compute the same homogeneous isotropic flow at increasing values of Re with fixed $Sc = 1$. The present paper deals with a complementary issue: by keeping Re and Sc fixed, our contribution will be to extend the analysis to wall-bounded turbulent flows.

Passive scalar fields in the neighbourhood of solid boundaries have been considered by Salman and Haynes (2007) and Boffetta et al. (2009). They employed a Lagrangian particle-tracking technique to describe decay or persistency of scalar concentration in peripheral regions of a two-dimensional synthetic flow, and of a plane Couette flow. Here, we consider the pressure-driven turbulent plane channel flow, which is considered as the simplest prototypical wall flow that offers at the same time a simple geometry and the physical features of more complex wall-bounded flows, and following Schumacher et al. (2005) and Watanabe and Gotoh (2007) we ask ourselves the same question about the existence and role of very small scales in the scalar field.

The aim of the present paper is thus to show that the spatial resolution adopted in past DNS studies of wall turbulence with passive scalar does not resolve an important range of very small yet dynamically significant micro-scales, which are responsible for the extremely intermittent nature of the scalar field. To demonstrate this statement, three DNS of the same channel flow at different spatial (and consequently temporal) resolutions are carried out. The lowest resolution corresponds roughly to the standard spatial resolution adopted in the past for most passive scalar studies: it is of the order of a few wall units, and comes from using for the passive scalar the spatial resolution typically employed for the velocity field. This spatial resolution is larger than $\langle\eta_B\rangle$. Our most resolved simulation, on the other hand, possesses a spatial resolution that goes well below the $\langle\eta_B\rangle$ level. The effects of varying resolution on the statistical features of the scalar field can thus be addressed, and their change with the wall distance described.

In particular, the focus of the present paper will be on the correct representation of the scalar dissipation. The dissipation ϵ_θ of the scalar variance is defined as:

$$\epsilon_\theta = 2\gamma \sum_{i=1}^{3} \left(\frac{\partial \theta'}{\partial x_i}\right)^2, \tag{2}$$

where $\theta' \equiv \theta - \langle\theta\rangle$ is the fluctuation of the passive scalar about the local mean. Of course ϵ_θ is particularly sensitive to the smallest scales of motion: it is known that ϵ_θ possesses very fine spatial structure (Schumacher et al., 2005), high internal intermittency, and significant small-scale anisotropy (Warhaft, 2000). In addition to being a suitable indicator of the smallest scalar motions, ϵ_θ is significant in many physical processes which are central in both industrial and environmental fields. A correct modeling of both integral- and micro-scale scalar dissipation features can, for example, establish whether a chemical reaction occurs or not, or enable the correct prediction of quantitative features of environmental pollution and to establish appropriate safety thresholds.

The outline of the paper is as follows: In Section 2, the characteristics of the numerical method will be briefly outlined; its validation will be discussed in Section 2.1 by reproducing the results of a channel flow DNS performed by Johansson and Wikström (1999). In Section 3, the numerical parameters employed in the simulations will be introduced, with a view to comparing between the spatial resolutions used here and the typical resolution employed in the past. The main results will then be presented, illustrating first in Section 4 the effects of the spatial resolution on integral-scale scalar quantities (mean profile and variance of scalar dissipation) and then in Section 5 the effects of varying resolution on the micro-structural features of the scalar field. Finally, a brief summary and some conclusive remarks will be given in Section 6.

2. The numerical method

The DNS code employed in this work has been developed from the pseudo-spectral, mixed-discretization, parallel algorithm introduced by Luchini and Quadrio (2006) for the DNS of the velocity field for wall-bounded turbulent flows. The extension of the original code to include the dynamics of a passive scalar has been implemented with the key requirement of keeping the same parallel strategy, and thus retaining the same computational efficiency. Since the wall-normal velocity and wall-normal vorticity formulation is used for the momentum equations, the evolutive equation for the passive scalar:

$$\frac{\partial \theta}{\partial t} + u_i \frac{\partial \theta}{\partial x_i} = \gamma \frac{\partial^2 \theta}{\partial x_i \partial x_i}, \tag{3}$$

is written to be formally identical to the wall-normal vorticity equation.

We indicate with x, y and z the streamwise, wall-normal and spanwise directions respectively. The corresponding velocity components are u, v and w and the passive scalar is θ. The computational domain has extensions $L_x, L_y = 2h$ and L_z in the corresponding directions. The friction Reynolds number Re_* is based on the channel half-width h, on the fluid's kinematic viscosity ν and on the friction velocity u_*, and is defined as $Re_* = u_* h/\nu$. The scalar concentration is expressed through the Schmidt number $Sc = \nu/\gamma$.

A Fourier expansion is used in the homogeneous directions, whereas fourth-order accurate, explicit compact finite-difference schemes are used to compute derivatives in the y direction. The number of discretization modes (points) is indicated with N_x, N_y and N_z. The collocation points in the near-wall direction are smoothly stretched from the wall to the centerline. Full dealiasing is used in the homogeneous directions. The time-integration algorithm uses a third-order Runge-Kutta scheme for the computation of the convective non-linear terms and a second-order Crank-Nicholson scheme for the evaluation of the viscous-implicit terms.

The flow in the channel is driven by a constant mean pressure gradient applied in the streamwise direction. Boundary conditions in the homogeneous directions are periodic whereas at the walls, no-slip and no-penetration conditions are imposed to the velocity field, and θ is set to a constant value. A mean scalar gradient is thus established between the two walls, ensuring a mean passive scalar

profile in the wall-normal direction. This boundary condition for the passive scalar has been already employed for example by Kim and Moin (1989), Johansson and Wikström (1999) and Kawamura et al. (2000). It is worth mentioning here that an alternative boundary condition can be used, that consists in imposing a constant scalar flux at each wall. Such a boundary condition has been chosen, for example, by Kasagi et al. (1992), Kasagi and Ohtsubo (1993), Kawamura et al. (1998, 1999). The differences between the two boundary conditions have been addressed by Kawamura et al. (2000): they show that scalar statistics, such as the mean profile, the root-mean-square fluctuation and the turbulent flux, are basically unchanged in the near-wall region, while they differ in the core region due to the either zero or non-zero mean scalar gradient in the channel's mid plane.

2.1. Validation

The numerical code is validated by replicating the DNS of a turbulent channel flow with passive scalar carried out by Johansson and Wikström (1999). This simulation is at $Re_* = 265$ and $Sc = 0.71$, with $L_x = 4\pi h$ and $L_z = 5.5h$, and with the spatial resolution determined by $N_x = 256$, $N_y = 193$ and $N_z = 192$, as in the original reference. After reaching a statistically steady state, our numerical simulation is continued for an overall averaging time of 4000 viscous time units, and 60 statistically time-independent flow fields are periodically written to disk for further analysis.

Fig. 1 compares the present results to what has been obtained by Johansson and Wikström (1999). The two simulations are compared in terms of wall-normal profiles of the mean scalar $\langle\theta\rangle^+$, the root-mean-square value σ_θ^+ of its fluctuations, and the mean scalar dissipation $\langle\epsilon_\theta\rangle^+$. The superscript '+' indicates a non-dimensional quantity after scaling with wall (inner) variables. The inner velocity scale is given by the friction velocity $u_* = (\tau_w/\rho)^{1/2}$, where τ_w and ρ are respectively the wall-shear stress and the fluid density, and the inner time scale t_* is defined by $t_* = \nu/u_*^2$. For the passive scalar field, the inner scale θ_* is given by:

$$\theta_* = \frac{\gamma}{u_*}\left.\frac{\mathrm{d}\langle\theta\rangle}{\mathrm{d}y}\right|_w,$$

where the subscript w indicates a derivative evaluated at the wall.

Given the definition (2) of the dissipation of scalar variance, its relevant scaling quantity ϵ_* is:

$$\epsilon_* = \frac{\gamma}{Sc}\left(\left.\frac{\mathrm{d}\langle\theta\rangle}{\mathrm{d}y}\right|_w\right)^2.$$

A close inspection of Fig. 1 establishes the agreement between the output of the present numerical tool and the results obtained by Johansson and Wikström (1999). The collapse of the curves is such that only for σ_θ^+ and $\langle\epsilon_\theta^+\rangle$ in the very proximity of the channel's centerline can the two simulations be discerned. This small residual difference is most probably due to the different time span used for computing statistics, that is not mentioned by Johansson and Wikström (1999).

3. Computational parameters

The present work focuses on the smallest scales of motion, and thus the available computational resources are best spent on spatial resolution. As a consequence, our simulations have neither particularly high values of Re_* and Sc, nor particularly large sizes of the computational box. Its dimensions are set at $L_y = 2h$, $L_x = 4.19h$ and $L_z = 2.09h$. The value of the friction Reynolds number is set at $Re_* = 160$. The value of the Schmidt number is set as $Sc = 1$, so that, according to Eq. (1), the mean Kolmogorov and Batchelor length-scales are identical.

Three DNS at increasing spatial resolution are carried out. They are labelled with **L**, **M** and **H** throughout the paper, to indicate **L**ow, **M**edium and **H**igh resolution. The parameters defining the discretization of the three simulations are summarized in Table 1. The grid spacings are expressed, as usual in wall turbulence, in viscous wall units, but they are also reported in terms of $\langle\eta_B\rangle_w$, the mean Batchelor length scale evaluated at the wall.

The temporal discretization is adapted to the spatial discretization, so that the time step used in simulation **H** is the finest. The overall averaging time (2400 viscous time units) and the number of statistically time-independent flow fields (60) stored on disk for further analysis for each of the three simulations are, however, left unchanged for all the simulations.

The spatial resolution of simulation **L** is comparable to the resolutions employed in most wall-turbulence DNS performed to date with passive scalars (Kawamura et al., 1998; Kawamura et al., 1999; Johansson and Wikström, 1999). Such a spatial resolution is usually considered to be adequate as far as the velocity field is concerned (Moin and Mahesh, 1998).

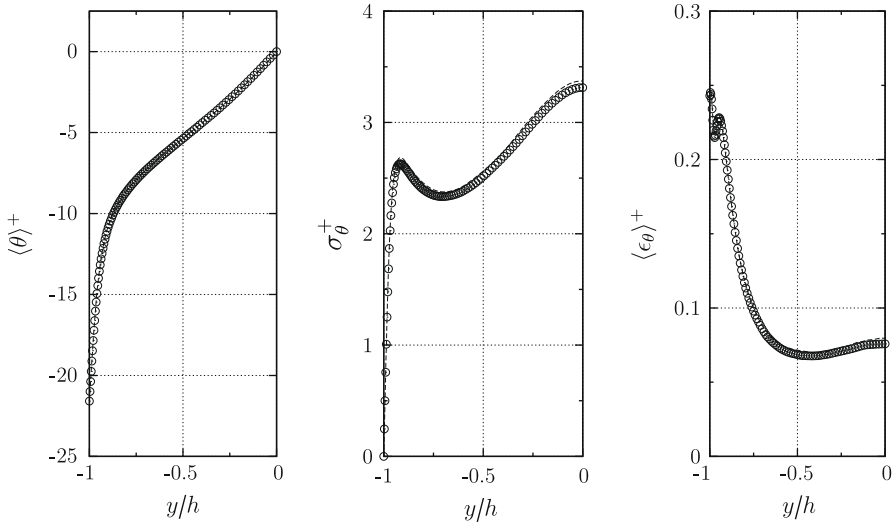

Fig. 1. Comparison between the present simulation (symbols) and the results by Johansson and Wikström (1999) (dashed line) for $Re_* = 265$ and $Sc = 0.71$. All quantities in inner units. Left: wall-normal distribution of the mean passive scalar. Center: wall-normal profile of the r.m.s. value of the passive scalar fluctuations. Right: wall-normal mean profile of the dissipation of scalar variance.

Table 1
DNS parameters: grid spacings Δx, Δy, Δz are expressed in terms of $\langle\eta_B\rangle_w$, the mean value of the Batchelor scale at the wall. In terms of viscous wall units, at the wall $\langle\eta_B\rangle_w^+ = 1.6$.

Simulation	**L**ow	**M**edium	**H**igh
N_x	64	340	680
N_z	64	170	340
N_y	128	128	256
$\Delta x/\langle\eta_B\rangle_w$	6.54	1.23	0.62
$\Delta z/\langle\eta_B\rangle_w$	3.28	1.23	0.62
$\Delta y_{min}/\langle\eta_B\rangle_w$	0.54	0.54	0.27
$\Delta y_{max}/\langle\eta_B\rangle_w$	2.47	2.47	1.24
Δx^+	10.46	1.97	1.00
Δz^+	5.25	1.97	1.00
Δy^+_{min}	0.86	0.86	0.43
Δy^+_{max}	3.95	3.95	1.98

On the other hand, simulation **H** has the highest resolution: owing to the increase with y of the lengthscale $\langle\eta\rangle$, that equals $\langle\eta_B\rangle$ since $Sc = 1$, the grid spacings Δx, Δz and Δy are consistently smaller than $\langle\eta_B\rangle$ in the whole wall-normal range. Still, motions at scales smaller than $\langle\eta_B\rangle$ do exist. Fig. 2 reports the statistical distribution of η_B, calculated employing Eq. (1) and the full definition of the dissipation rate ϵ of turbulent kinetic energy. The probability density function of η_B is measured at a few wall-normal locations, and it is compared to the spatial resolution of simulation **H** at the same y positions. It turns out that even the simulation employing the finest resolution might be only marginally resolved. At each wall-normal distance shown, in fact, either the streamwise (or spanwise) grid spacing, which is set constant to one wall unit throughout the channel, or the wall-normal spacing, that smoothly increases from the wall to the centerline, is larger than the smallest values locally assumed by η_B. As a further means to assess the validity of the spatial discretization, the resolution criterion introduced by Donzis et al. (2008) has been used to tentatively compute an error bound for the three spatial derivatives involved in the definition of ϵ_θ, Eq. (2). Although the criterion applies to homogeneous and isotropic turbulence only, its use for simulation **H** and at the channel centerline, where the flow is expected to approach local isotropy, indicates an error of 0.14% for the streamwise and spanwise derivatives, and an error of 0.71% for the wall-normal derivative.

The spatial resolution of simulation **M** is midway between **L** and **H**. Note that the streamwise and spanwise spatial resolution of case **M**, when expressed in terms of $\langle\eta_B\rangle_w$, is finer than the highest resolution employed in past DNS of passive scalar turbulent channel flows with $Sc \geqslant 1$ we are aware of. In absolute terms, this is the study recently carried out by Schwertfirm and Manhart (2007) whose finest grid spacings are $\Delta x^+ = 0.68$, $\Delta z^+ = 0.85$ and $0.18 \leqslant \Delta y^+ \leqslant 0.75$. Their DNS, however, was aimed at investigating flows with high values of the Schmidt number, so that the resulting spatial resolution evaluated in terms of the Batchelor scale is rather coarse: $\Delta x/\langle\eta_B\rangle_w = 3.09$, $\Delta z/\langle\eta_B\rangle_w = 3.86$ and $0.82 \leqslant \Delta y/\langle\eta_B\rangle_w \leqslant 3.41$.

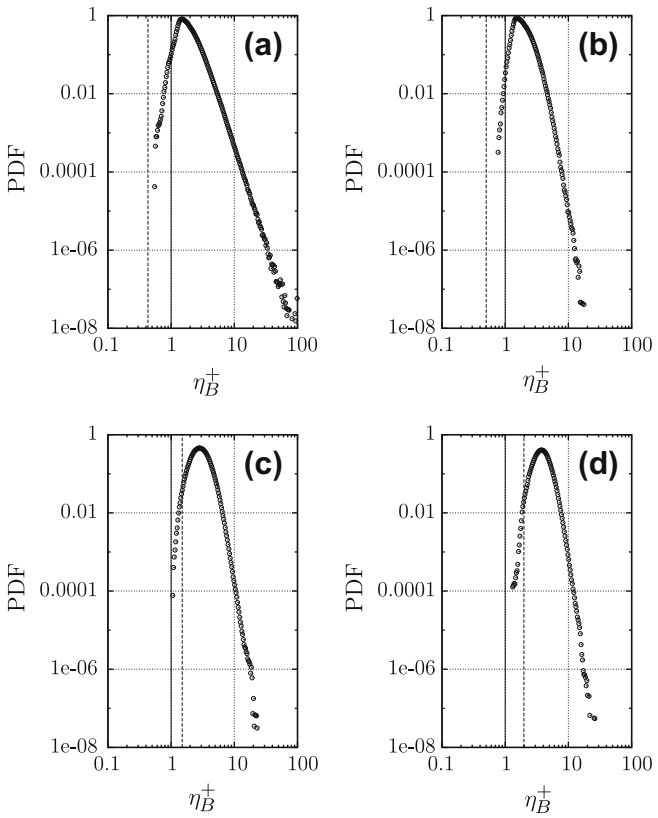

Fig. 2. Probability density functions of η_B^+ for: (a) $y^+ = 0$; (b) $y^+ = 5$; (c) $y^+ = 73$; and (d) $y^+ = 160$. The vertical lines indicate the spatial resolution of simulation **H**: the continuous vertical line is $\Delta x^+ = \Delta z^+ = 1$, whereas Δy^+ is shown as a dashed vertical line, and increases with y.

4. Statistical moments of ϵ_θ

The lowest-order statistical moments of the scalar dissipation ϵ_θ are considered first. Fig. 3 shows the wall-normal distribution of statistical moments of ϵ_θ, respectively of order one (the mean profile) and order two (the variance), computed at different spatial resolutions. Since the wall scale ϵ_* used to express $\langle\epsilon_\theta\rangle$ and $\sigma^2_{\epsilon_\theta}$ in wall units is found to be resolution-dependent, showing a difference of up to 5% between simulation **L** and **H**, in this and in the following figure each dataset is made non-dimensional through its corresponding wall scale ϵ_*.

It can be easily appreciated how neither simulation **L** nor simulation **M** have the spatial resolution required to compute these non-local quantities in a mesh-independent way. Indeed, a complete overlap between curve **H** and curve **M** cannot be observed, and thus even simulation **H** might still be slightly under resolved to correctly capture the full details of the fluctuations of ϵ_θ.

The three curves for $\langle\epsilon_\theta\rangle^+$ in Fig. 3 (left) do not overlap in the whole y^+ range, if exception is made for the near-wall region (say for $y^+ < 7$), indicating that only in proximity of the wall case **L** possesses enough resolution to represent $\langle\epsilon_\theta\rangle$ correctly. Moving

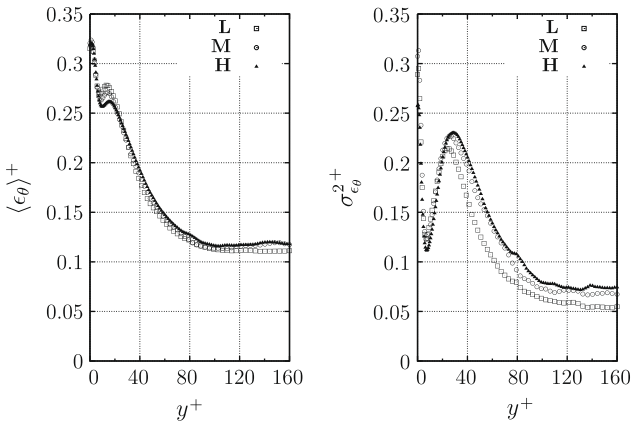

Fig. 3. Effects of the spatial resolution on the mean wall-normal distribution of the scalar dissipation rate ϵ_θ (left) and on its variance $\sigma^2_{\epsilon_\theta}$ (right).

towards the central region of the channel, the differences among the three curves become evident, especially in the buffer-layer ($10 < y^+ < 30$) where the separation is significant and a change larger than 7% in the prediction of the mean value is observed. In this region, simulation **H** predicts lower absolute values of $\langle \epsilon_\theta \rangle$, suggesting that on average the (absolute value of) dissipation of scalar variance associated to the finest scalar structures is lower. In the log-layer and in central region of the channel, only the curves corresponding to simulations **M** and **H** collapse, indicating that in this region the spatial resolution of simulation **M** is enough to describe the mean scalar dissipation field.

Spatial resolution effects appear to be more relevant when the variance of ϵ_θ is considered: in Fig. 3 (right) the three curves remain separate for the whole y^+ range.

It is important to note how the same analysis carried out for the dissipation rate ϵ of turbulent kinetic energy shows that these effects are substantially peculiar to the ϵ_θ field. Fig. 3 should be compared with Fig. 4, which shows the wall-normal profiles of the first two statistical moments of ϵ. Though small resolution effects can still be observed, particularly between cases **L** and **M**, it clearly emerges that the passive scalar field is characterized by a much finer and intermittent structure than the underlying velocity field (Warhaft, 2000). Hence turbulent flows with passive scalar, even at $Sc = 1$ and $\langle \eta_B \rangle = \langle \eta \rangle$, present resolution requirements for correctly investigating non-local quantities of the scalar field which are more demanding than those required for the velocity field. When these requirements are not fully met, the insufficient resolution causes sizeable errors in the prediction of scalar-related mean quantities.

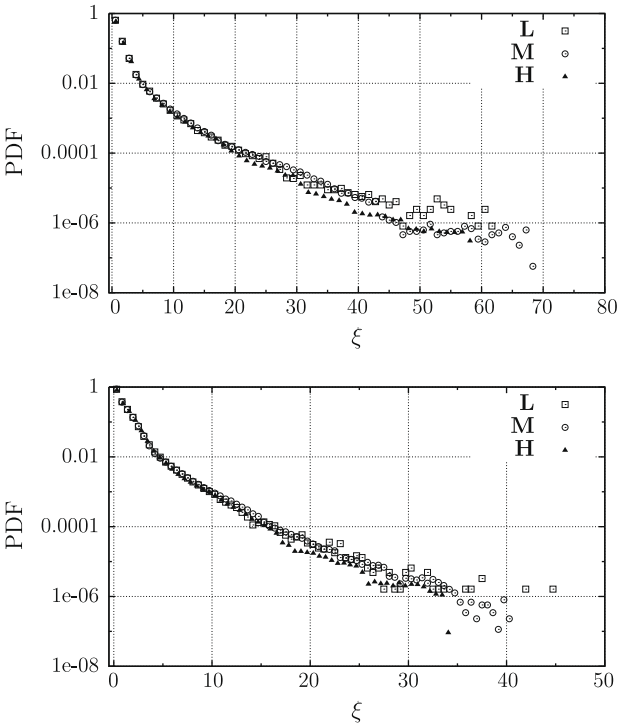

Fig. 5. PDF of $\xi = \epsilon_\theta / \langle \epsilon_\theta \rangle$ for two wall-normal positions at $y^+ = 0$ (top) and $y^+ = 5$ (bottom).

5. PDF of ϵ_θ

In this section, the resolution effects already observed in terms of non-local quantities are discussed in terms of their intensity distribution. We consider first in Section 5.1 particularly intense dissipation events, i.e. events characterized by extreme values of ϵ_θ, and examine how the spatial resolution affects the right tail of the probability density function of the quantity $\xi = \epsilon_\theta / \langle \epsilon_\theta \rangle$. Then in Section 5.2 the same analysis is carried out for weak events (i.e. events for which $\xi \ll 1$) by looking at the left tail of the probability density function of ξ.

5.1. Strong dissipative events

Fig. 5 shows the probability density function of the quantity $\xi = \epsilon_\theta / \langle \epsilon_\theta \rangle$ computed at $y^+ = 0$ (i.e. at the wall) and $y^+ = 5$ (in the viscous sub-layer). Both the low-resolution simulations **L** and **M** are characterized by PDF with wide tails, which appear to shrink when the spatial resolution is increased in case **H**. In the viscous sub-layer, in particular, the length of the right tails of the PDF curves is observed to increase as the spatial resolution is reduced. This implies that, in the near-wall region, extremely intense events, that are present in cases **L** and/or **M**, disappear in simulation **H**. The limited spatial resolution of case **L** also results in overestimating events of intermediate intensity.

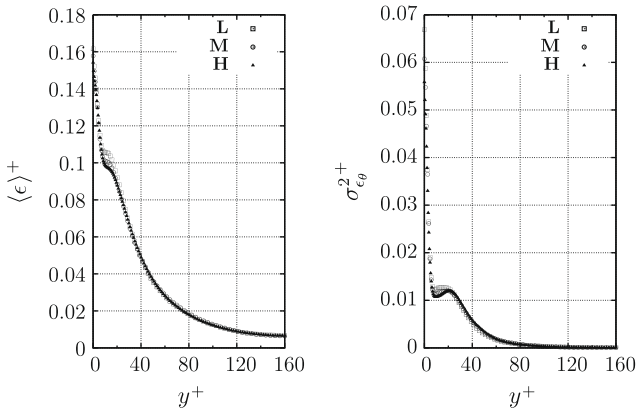

Fig. 4. Effects of the spatial resolution on the mean wall-normal distribution of the turbulent kinetic energy dissipation rate ϵ (left) and on its variance σ^2_ϵ (right).

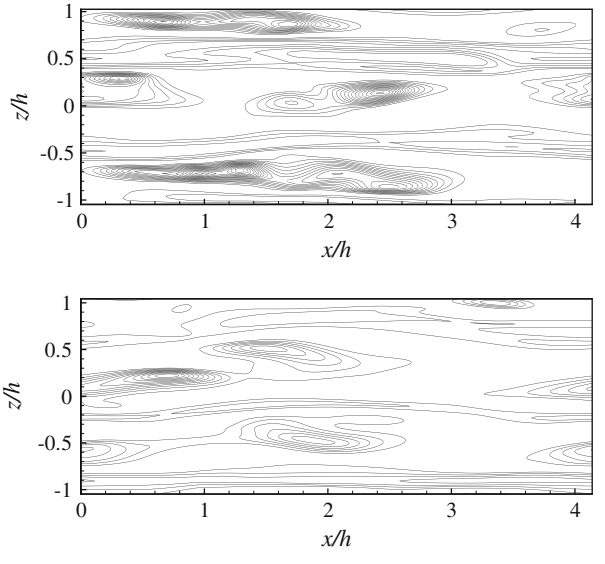

Fig. 6. Two-dimensional instantaneous wall-parallel cuts of the scalar dissipation field ϵ^+_θ for $y^+ = 0$ for simulation **L** (top) and **H** (bottom). Levels from 0 by 0.25 increments. Maxima are 4.15 (top) and 2.98 (bottom).

These conclusions, based on statistical quantities, can be arrived at by also observing instantaneous snapshots of the ϵ_θ field. In particular, a wall-parallel section of the computational domain taken at $y = 0$ (i.e. at the wall) is shown in Fig. 6, where the morphology of an ϵ_θ field computed with the lowest (top) and the highest (bottom) resolutions are compared. The qualitative differences between the two slices help explaining the separation of the curves observed above in the context of Fig. 5. Case **L** always shows a larger number of regions with intense ϵ_θ; their size is larger when compared to the analogous structures observed in case **H**. Furthermore, the typical values of ϵ_θ for events of extreme intensity appears to be larger in simulation **L**. In this pair of snapshots, for example, the instantaneous maximum of ϵ_θ^+ is 4.15 for case **L** and 2.98 for case **H**. Analogous characteristics can be observed in wall-parallel cuts taken through the viscous sub-layer.

The pattern just described, i.e. one where marginal resolution tends to overemphasize extreme dissipations, reverses when the attention is shifted from the near-wall region to the logarithmic layer and the central region of the channel. Fig. 7 reports again the PDF of ϵ_θ, this time computed at $y^+ = 73$ and $y^+ = 160$ (channel centerline). Here the most intense scalar dissipation events are reliably predicted by the highest spatial resolution only. This feature is more evident in the log-layer, where the tails of the probability density functions corresponding to cases **M** and **H** are definitely longer than the tail of the curve for case **L**. Moreover, in the log-layer, the intensity of the strongest events captured by the simulation increases with the adopted spatial resolution, as evident from the length of the PDF tails. This implies that resolution **M** is certainly inadequate to capture the most intense scalar dissipation events in the log layer, and the same might be true for case **H** too. At the channel centerline, the separation between the PDF tails becomes smaller, yet case **L** is evidently not capable of capturing the strongest events.

Again, a look at instantaneous fields of ϵ_θ in wall-parallel planes confirms these remarks. Fig. 8 shows sections at $y^+ = 160$ for simulations **L** and **H**, and shows how the resolution of case **L** does not represent the ϵ_θ field correctly, owing to its extremely intermittent spatial structure. The maxima of ϵ_θ^+ in these two particular slices are 1.65 (case **L**) and 4.35 (case **H**).

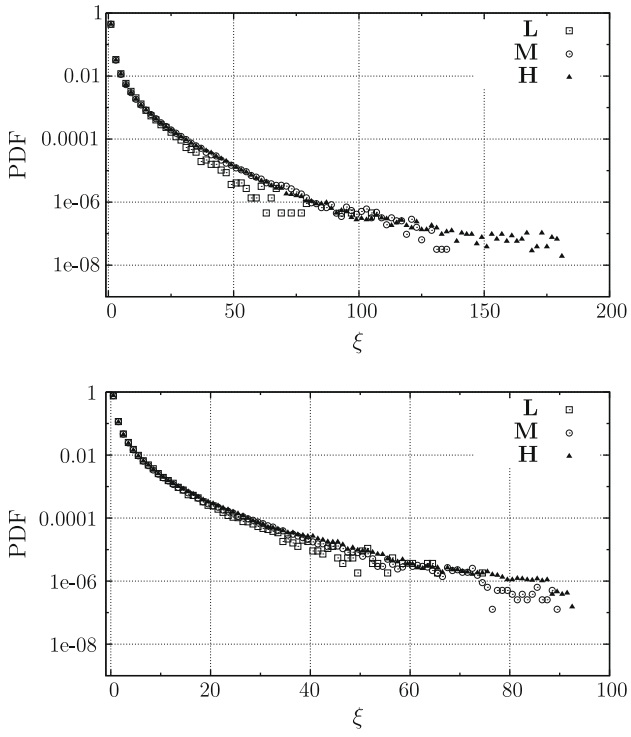

Fig. 7. PDF of $\xi = \epsilon_\theta / \langle \epsilon_\theta \rangle$ for two wall-normal positions at $y^+ = 73$ (top) and $y^+ = 160$ (bottom).

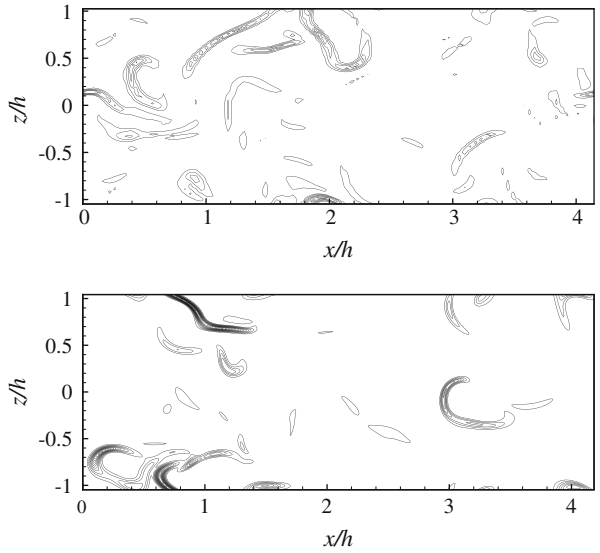

Fig. 8. Two-dimensional instantaneous wall-parallel cuts of the scalar dissipation field ϵ_θ^+ for $y^+ = 160$ for simulation **L** (top) and **H** (bottom). Levels from 0 by 0.25 increments. Maxima are 1.65 (top) and 4.35 (bottom).

5.2. Weak dissipative events

Fig. 9 shows the PDFs of the quantity ξ for the three different simulations in the near-wall region and in the log-layer. The choice of this quantity and the logarithmic scale used on the horizontal axis, emphasize the left side of the PDF, and highlight the effects of the spatial resolution on the weakest dissipation events.

The emerging pattern is that the left tail of the PDF for case **L** is consistently shorter than the tails for the other simulations. This means that a marginal spatial resolution is not capable to identify extremely weak events of scalar dissipation. As already observed by Schumacher et al. (2005), this can be explained by the fact that numerical simulations with poor resolution are characterized by relatively high noise (when compared to more resolved simulations) and this implies a lower signal-to-noise ratio. The noise becomes particularly significant in the regions of low-magnitude ϵ_θ

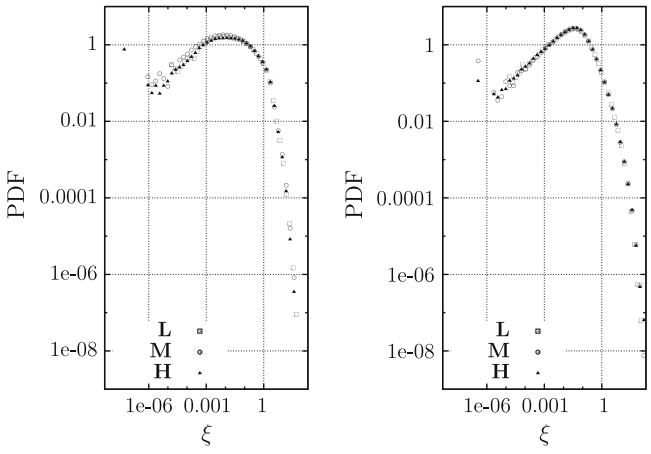

Fig. 9. PDF of $\xi = \epsilon_\theta / \langle \epsilon_\theta \rangle$ for $y^+ = 5$ (left) and $y^+ = 73$ (right).

events, that end up being covered by the noise floor. It should be observed, moreover, that our focus here is on extremely weak events, that are revealed by properly resolved simulations through wider left tails of the PDF, whereas other studies of isotropic turbulence (Schumacher et al., 2005; Watanabe and Gotoh, 2007) considered events of relatively larger intensity, for which a poor resolution implies underestimation of the PDF.

Simulations **M** and **H**, on the other hand, show no dissimilarities as far as the weakest ϵ_θ events are considered, if exception is made for the viscous sub-layer (see again Fig. 9), where the highest resolution is needed to observe the smallest events.

Looking at the same quantities in the central region of the channel (not shown) confirms these observations, whereas at the wall, on the opposite, the three curves essentially coincide at small ξ. This last observation is explained both by the iso-scalar boundary condition employed in the present work (which implies, tendentially, a uniformity of the scalar field in wall-parallel planes for very small wall distances) and by the larger characteristic length scale of the ϵ_θ structures in the near-wall region, which can therefore be represented with lower spatial resolution.

6. Discussion and conclusions

In the present work, three Direct Numerical Simulations of a passive scalar in turbulent channel flow have been carried out at different spatial resolutions. The aim was to investigate the effects of the spatial resolution on the statistical features of the flow, and to describe their change with the distance from the wall. We have centered our analysis on the statistical description of the scalar dissipation ϵ_θ. Grid-dependent results have been observed not only in the statistical description of the passive scalar's micro-structure, but – more surprisingly – also in its integral-scale characteristics, unless the grid spacing in all the three directions is smaller than the local value of the Batchelor length scale.

The wall-normal profiles of $\langle\epsilon_\theta\rangle$ and its variance show that, due to the strong coupling between large-scale advective motions and small-scale molecular diffusive mixing, the most resolved DNS is needed even for the correct description of such integral-scale quantities. The required resolution goes far beyond what has been routinely adopted in the past for similar simulations. The resolution requirements become of course more stringent as soon as the order of the considered statistical moments increases. A comparison between the wall-normal mean profiles of ϵ_θ and its variance with the corresponding profiles for the dissipation rate of turbulent kinetic energy strongly suggests that such strict requirements concern primarily the passive scalar, owing to its distinctive intermittent character.

Extra-fine spatial resolution becomes essential when the smallest scales of the passive scalar are the main feature one is interested in. The PDF of ϵ_θ fluctuations, measured in the channel's log-layer and the mid plane and discussed in Sections 5.1 and 5.2, do in fact show that the range of scales which are not resolved by standard spatial resolutions is responsible for the extremely intermittent nature of the passive scalar field, that is observed for both very weak and very intense scalar dissipation events. This is consistent with the pattern described by Schumacher et al. (2005) and Watanabe and Gotoh (2007) for homogeneous isotropic turbulence. When the wall is approached, however, the influence of the solid boundary reverses the picture in the context of strong dissipative events. In this region of the flow we have shown how the incomplete representation of the smallest scales leads to a significant overestimate of the strongest ϵ_θ events, so that the extremely intermittent nature of the passive scalar field is not correctly predicted. Underestimating the fluctuations of the scalar field in proximity of solid boundaries may lead, in the context of environmental issues, to a dangerous underestimation of the concentration of pollutants in regions close to the ground, consistently with the picture outlined by Boffetta et al. (2009).

It is puzzling to observe how the effects of insufficient resolution change in nature when moving from the centerline down to the wall. These varying effects are related to the role played by the solid walls, the iso-scalar boundary conditions, the changes throughout the channel of the morphology and the structure of both the scalar fluctuation field θ' and the scalar dissipation field ϵ_θ. The evolution of the morphology of the scalar dissipation field ϵ_θ as the distance from the wall increases can be observed by comparing Figs. 6 and 8 with the contribution of Fig. 10. The relatively large, high-dissipation structures which are noticed in near-wall horizontal sections of the flow field (visualized in Fig. 6) do disappear as the distance from the wall increases, and are replaced by thin and elongated structures (shown in Fig. 8) which recall, as it could have been expected, the structures observed by Brethouwer et al. (2003) and Schumacher et al. (2005) in homogeneous and isotropic turbulence. According to these papers, the thin and elongated structures are twisted, folded, very close and almost parallel to each other, and are most likely cross-sections of the sheet-like structures of ϵ_θ which can be observed in the three-dimensional visualization of the scalar dissipation field plotted in Fig. 10. The latter clearly shows the important role played by the walls in the morphology of the scalar dissipation field, whose sheet-like structures are forced to be predominantly parallel to the walls in the near-wall region, while in the central region of the channel their orientation is free to assume more of an isotropic character.

The iso-scalar boundary condition does, on the other hand, play a key role in the evolution of ϵ_θ's nature throughout the channel. The boundary conditions are responsible for the vanishing horizontal gradients of θ' at the walls. Therefore, in this region, the unique non-zero contribution to ϵ_θ comes from wall-normal gradients of θ'. For simulations with lower spatial resolution, values of θ' at larger wall-normal distances, where the passive scalar field is more fluctuating, are involved in the numerical evaluation of wall-normal gradients, that consequently result overestimated. This last feature is quantitatively described by Fig. 11, where the probability density function of θ'^+ is plotted at two different values of y^+, corresponding to the points nearest to the wall for simulation **H**, at $y^+ = 0.431$, and simulation **L**, at $y^+ = 0.871$. Indeed, much wider

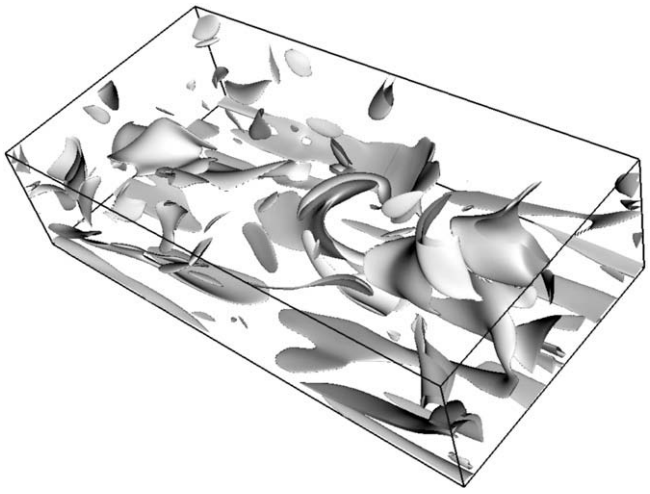

Fig. 10. Three dimensional visualization of iso-scalar dissipation surfaces corresponding to $\epsilon_\theta^+ = 0.73$ in the bottom half of the channel.

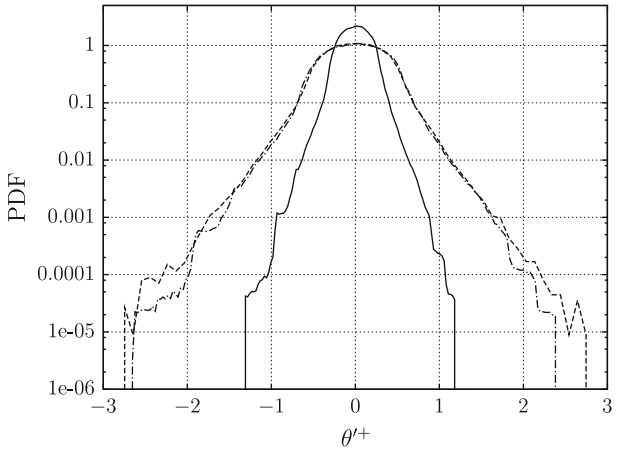

Fig. 11. Probability density function of $\theta'^{+} = \theta'/\theta_*$ at the point nearest to the wall for case **H** (continuous line, $y^+ = 0.431$) and case **L** (dashed line, $y^+ = 0.871$). The dash-dotted line represents the wall-normal position $y^+ = 0.871$ for simulation **H** (i.e. the second inner point), and shows how a coarser resolution predicts extreme events with larger intensity.

exponential tails of the PDF of θ'^{+} are observed further from the wall. To explain the steeper θ' wall-normal gradients computed at the wall by simulation **L**, the same figure also plots the PDF of θ'^{+} from simulation **H** at $y^+ = 0.871$. This allows a direct comparison of the PDF computed at the same physical distance from the wall, for different resolutions, and confirms how scalar gradients tend to be overestimated by poor resolution, since wider tails of the PDF are predicted by case **L**. Moreover, events of extreme intensity appear more frequently. It is worth noting that the value of the quantity θ_*, employed to make the scalar fluctuation field dimensionless in Fig. 11, changes slightly from case **L** to case **H**. This produces a shrink of the PDF for case **L** and slightly reduces the overestimation effect.

The described properties of the scalar fluctuation field θ' in the near-wall region (strongly determined by the iso-scalar boundary condition) do not characterize anymore the fluctuation field in the channel's log-layer and in the central region of the channel. The structure of θ' in these regions presents non-zero horizontal gradients which are steep and localized due to the intermittent nature of the passive scalar field, which, as already discussed, increases with the distance from the wall. In addition, this scalar intermittency is coupled to a very fine spatial structure and this explains why in the logarithmic layer and near the mid plane of the channel intense ϵ_θ events are underestimated by simulation **L**.

The (at least partial) grid-dependency presented by several results discussed throughout this paper implies that even the highest spatial resolution employed (simulation **H**) could be only marginally adequate. This is also suggested by the comparison, carried out in Fig. 2, between the statistical distribution of the Batchelor's scale η_B and the spatial resolution of case **H** in the different layers of the channel flow. Grid resolutions finer than the smallest local value of η_B will therefore be required to investigate small-scale features of passive scalar mixing in wall-bounded turbulent flows.

Acknowledgements

A. Johansson is gratefully acknowledged for having shared with us his data. LG has been partially supported by a PRIN 2005 grant on *Large-scale structures and wall turbulence*. P. Luchini at Università di Salerno is thanked for his continuous support and for the use of computing time.

References

Boffetta, G., De Lillo, F., Mazzino, A., 2009. Peripheral mixing of passive scalar at small Reynolds number. J. Fluid Mech. 624, 151–158.
Brethouwer, G., Hunt, J., Nieuwstadt, F., 2003. Micro-structure and Lagrangian statistics of the scalar field with a mean gradient in isotropic turbulence. J. Fluid Mech. 474, 193–225.
Chen, S., Cao, N., 1997. Anomalous scaling and structure instability in three-dimensional passive scalar turbulence. Phys. Rev. Lett. 78 (18), 3459.
Donzis, D.A., Yeung, P.K., Sreenivasan, K.R., 2008. Dissipation and enstrophy in isotropic turbulence: resolution effects and scaling in direct numerical simulations. Phys. Fluids 20, 45108.
Johansson, A.V., Wikström, P., 1999. DNS and modelling of passive scalar transport in turbulent channel flow with a focus on scalar dissipation modelling. Flow Turbul. Combust. 63, 223–245.
Kasagi, N., Ohtsubo, Y., 1993. Direct Numerical Simulation of Passive Scalar Field in a Turbulent Channel Flow. Turbulent Shear Flows, vol. VIII. Springer. pp. 97–119.
Kasagi, N., Tomita, Y., Kuroda, A., 1992. Direct numerical simulation of passive scalar field in a turbulent channel flow. Trans. ASME 114, 598–606.
Kawamura, H., Ohsaka, K., Abe, H., Yamamoto, K., 1998. DNS of turbulent heat transfer in channel flow with low to medium-high Prandtl number fluid. Int. J. Heat Fluid Flow 19, 482–491.
Kawamura, H., Abe, H., Matsuo, Y., 1999. DNS of turbulent heat transfer in channel flow with respect to Reynolds and Prandtl number effects. Int. J. Heat Fluid Flow 20, 196–207.
Kawamura, H., Abe, H., Shingai, K., 2000. DNS of turbulence and heat transport in a channel flow with different Reynolds and Prandtl numbers and boundary conditions. In: 3rd Int. Symp. Turbulence, Heat and Mass Transfer.
Kim, J., Moin, P., 1989. Transport of Passive Scalars in a Turbulent Channel Flow. Turbulent Shear Flows, vol. VI. Springer. pp. 85–96.
Luchini, P., Quadrio, M., 2006. A low-cost parallel implementation of direct numerical simulation of wall turbulence. J. Comp. Phys. 211 (2), 551–571.
Moin, P., Mahesh, K., 1998. Direct numerical simulation: a tool in turbulence research. Ann. Rev. Fluid Mech. 30, 539–578.
Mydlarski, L., Warhaft, Z., 1998. Passive scalar statistics in high-Peclet-number grid turbulence. J. Fluid Mech. 358, 135–175.
Salman, H., Haynes, P.H., 2007. A numerical study of passive scalar evolution in peripheral regions. Phys. Fluids 19 (6), 67101.
Schumacher, J., Sreenivasan, K., Yeung, P., 2005. Very fine structures in scalar mixing. J. Fluid Mech. 531, 113–122.
Schumacher, J., Sreenivasan, K.R., Yakhot, V., 2007. Asymptotic exponents from low-Reynolds-number flows. New J. Phys. 9 (89).
Schwertfirm, F., Manhart, M., 2007. DNS of passive scalar transport in turbulent channel flow at high Schmidt numbers. Int. J. Heat Fluid Flow 28, 1204–1214.
Shraiman, B., Siggia, E., 2000. Scalar turbulence. Nature 405, 639–646.
Sreenivasan, K., 1991. On local isotropy of passive scalars in turbulent shear flows. Proc. Roy. Soc. Math. Phys. Sci. 434 (1890), 165–182.
Sreenivasan, K.R., 2004. Possible effects of small-scale intermittency in turbulent reacting flows. Flow Turbul. Combust. 72, 115.
Sreenivasan, K., Antonia, R., 1997. The Phenomenology of small-scale turbulence. Annu. Rev. Fluid Mech. 29, 435–472.
Wang, L.-P., Chen, S., Brasseur, J., 1999. Examination of hypotheses in the Kolmogorov refined turbulence theory through high-resolution simulations. Part 2. Passive scalar field. J. Fluid Mech. 400, 163–197.
Warhaft, Z., 2000. Passive scalars in turbulent flows. Annu. Rev. Fluid Mech. 32, 203–240.
Watanabe, T., Gotoh, T., 2007. Inertial-range intermittency and accuracy of direct numerical simulation for turbulence and passive scalar turbulence. J. Fluid Mech. 590, 117–146.
Yakhot, V., Sreenivasan, K.R., 2005. Anomalous scaling of structure functions and dynamic constraints on turbulence simulations. J. Stat. Phys. 121, 823.
Yeung, P., Donzis, D., Sreenivasan, K., 2005. High Reynolds-number simulation of turbulent mixing. Phys. Fluids 17, 081703.